Theoretical limits for visibly transparent photovoltaics

Richard R. Lunt[a)]
Department of Chemical Engineering and Materials Science, Michigan State University, East Lansing, Michigan 48824, USA

(Received 31 March 2012; accepted 9 July 2012; published online 24 July 2012)

Transparent photovoltaics (PVs) provide a potentially facile route to building-integrated PVs and seamless energy-harvesting within non-window surfaces such as electronic displays, autonomously powered electronic-glazings, and mobile-electronic accessories. Such devices have been enabled by manipulation of excitons in organic and molecular semiconductors that allow for selective ultraviolet and near-infrared solar conversion. Here, the theoretical efficiency limits of transparent photovoltaics are determined as a function of transparency. Power-production from ultraviolet and near-infrared photons alone leads to a theoretical single-junction efficiency of 21% in transparent structures, compared to 33% for opaque-junctions. Reducing thermal losses via transparent multi-junction stacking these limits increase to 37%. © *2012 American Institute of Physics*. [http://dx.doi.org/10.1063/1.4738896]

The development of transparent photovoltaics (PVs) can enable seamless integration onto any already utilized transparent surfaces for PV deployment, such as on building windows, skylights, greenhouses, sun-roofs, and mobile electronic devices without requiring additional structural framing or acquisition of undeveloped real estate. In general, the purpose of windows and displays is to provide natural lighting or a clear view. This problem can be approached with the development of a visibly transparent PV technology that selectively harvests near-infrared (NIR) and ultraviolet (UV) light. A high level of visible transmittance (VT) on the order of 70%–80% for architectural and 55%–90% for automotive is necessary for ubiquitous adoption of solar-active windows.[1] Transparent solar cells designed for high-end device applications (e.g., mobile electronics integration) require even greater transparency >80%–90%, where display quality is paramount.

Recently, we have shown that by exploiting the excitonic character of molecular and organic semiconductors, it is possible to produce near-infrared PV architectures that are selectively absorptive in the UV and NIR, enabling visibly transparent active-layer photovoltaics for optimization of both efficiency and transparency.[2] These structures can also be added ubiquitously to non-transparent surfaces without affecting their underlying aesthetic, are capable of harvesting direct and indirect light, and could be combined with spatially distributed inorganic cells[3–5] or semitransparent devices[6–17] to further boost visible (VIS) external quantum efficiencies (EQEs) for niche applications with less stringent transparency requirements (e.g., façade, darkened, or colored glass applications). Although stringent transparency requirements could create challenges for full module scale-up in large-area applications due to bus bar integration necessary to reduce resistive losses,[18,19] this is likely surmountable with the recent development of highly transparent and highly conductive metal nanowire grids,[20–23] carbon nanotube meshes,[24] or improved transparent conducting oxides interconnects.[25]

In this article, the theoretical efficiency limits are determined as a function of transparency to define the maximum realizable goals for transparent single- and multi-junction photovoltaics in a range of applications. The range of perceptible visible light is first determined using color rendering index (CRI) analysis and subsequently utilized in determining thermodynamic efficiency limits for visibly transparent solar cells.

The CRI is a quantitative metric for evaluating the quality of lighting systems and can be utilized to evaluate the level or perceptible color-tinting of a window. CRIs are calculated based on ideal transmission profiles (step-functions) in combination with CIE 1976 three-dimensional uniform color space (CIELUV), CIE 1974 test-color samples, and with correction for chromatic adaptation (non-planckian-locus), when necessary, according to[26]

$$\mathrm{CRI} = \frac{1}{8}\sum_{i=1}^{8}\left(100 - 4.6\sqrt{(\Delta L_i^*)^2 + (\Delta u_i^*)^2 + (\Delta v_i^*)^2}\right), \quad (1)$$

where ΔL_i^*, Δu_i^*, and Δv_i^*, are the difference in lightness (L^*) and chromaticity coordinates (u^*,v^*) between each color sample, i (8 in total) "illuminated" with a fixed reference solar spectrum (AM1.5G) and the transmission sources ($T(\lambda)\cdot$AM1.5(λ)). The weighted average VT is calculated according to[26]

$$\mathrm{VT} = \frac{\int T(\lambda)P(\lambda)S(\lambda)d\lambda}{\int V(\lambda)S(\lambda)d\lambda}, \quad (2)$$

where λ is the wavelength, T is the transmission spectrum, P is the photopic response of the human eye, S is the solar energy flux, and the integration is preformed over a sufficient wavelength range to completely encompass P (e.g., 300–900 nm) so that it is accordingly independent of any defined visible wavelength range. Thermodynamic limiting efficiencies are calculated via the Shockley ideal diode equation with radiative-limited recombination dark current, viz,[27]

a)rlunt@msu.edu.

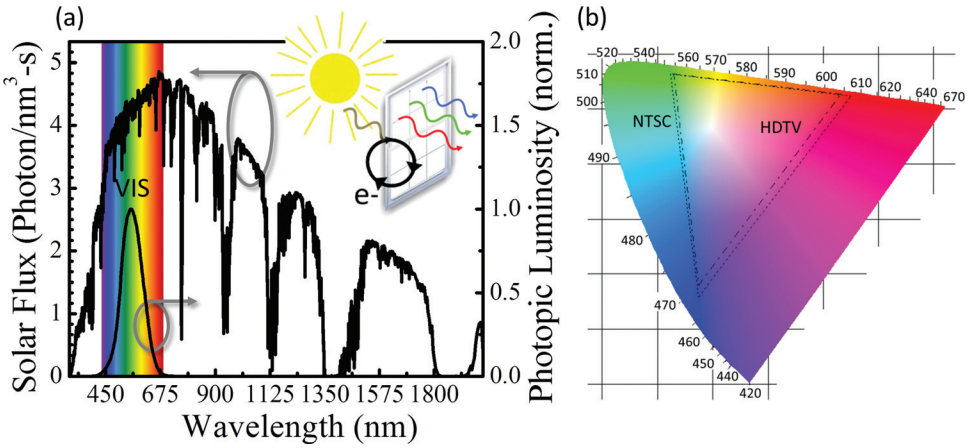

FIG. 1. (a) Solar photon flux (left axis) with the photopic response function (right axis) plotted versus wavelength. (inset) Schematic of a visibly transparent power-producing window. (b) CIE 1976 uniform chromaticity diagram with the locations of the red (R), green (G), and blue (B) emitters of the National Television System Committee (NTSC) and High-Definition Television (HDTV) display standards highlighted, where these systems roughly utilize 470 nm, 555 nm, and 605 nm for R, G, and B components, respectively, to generate full color displays.

$$J_S \cong qg \int_{E_G}^{\infty} \frac{E^2/EQE}{\exp(E/nkT) - 1} dE, \tag{3}$$

where $g = 2\pi/(c^2h^3)$, n is the ideality factor ($n = 1$ here), c is the speed of light, h is Planck's constant, and E_G is the active layer bandgap. For heterojunction devices, E_G is subsequently replaced in Eq. (3) with the interface gap, I_G, which is the difference between the highest occupied molecular orbital energy of the donor and the lowest unoccupied molecular orbital energy. Practical laboratory efficiencies (non-module) are then calculated as outlined in Ref. 28 for excitonic and nanostructured semiconductors capable of enabling transparent structures with fractional scaling of the Shockley-Queisser (SQ) voltage, photocurrent, and fill factor. This scaling estimates, *a-posteriori*, an upper limit voltage for heterojunction devices that accounts for replacing E_G with I_G that leads to increased dark-current recombination, and therefore decreasing voltage scaling, due to the heterojunction energy offset required to dissociate excitons.[29–33] Resistive losses for full module scale-up can be further considered (but was not applied here) by multiplying the practical laboratory efficiencies with an upper limit heuristic factor of ~0.75 typical for other thin-film PV scale-up.[28,34,35] Series-integrated tandem junction efficiencies are calculated by constraining current-density (J) matching in each cell at every voltage, $J(V) = J_i(V_i,E_i) = J_{i+1}(V_{i+1},E_{i+1})$. This equation was solved for the voltage in each cell (V_i) as a function of J, so that the total device voltage is $V = \sum V_i$.

In evaluating the efficiency limits of transparent photovoltaics, it is first necessary to define the range of the visible part of solar spectrum that should be transmitted and the spectral components that can be utilized for power generation. For example, the photopic response of the human eye is shown overlain with the solar spectrum in Figure 1. One assessment for the visible range is defined for a photopic response >0.1% peak sensitivity, resulting in a visible spectral range of 390–720 nm.[26] Here, we look for a visible range suitable for window integration that can maximize the contribution to the solar cell efficiency while minimizing any visual impact. We therefore look to sharp drop-offs in color rendering indices for transmitted AM1.5G (AM1.5G alone yields a CRI of 100) since the goal would be to offset lighting demands and avoid color-tinting. Shown in Figure 2 is the color rendering index and weighted VT calculated for ideal step-function transmission curves moved along the wavelength axis. Illumination sources are considered to be exceptional quality for CRI > 95, and of good quality between 70 and 90.[26] For a CRI ≥ 99, the visible range would be defined as 405–700 nm, which is close to the 0.1% peak sensitivity limit. For a CRI > 95, the range is determined as 435–670 nm (see Figure 2) with a corresponding VT > 99.5%. While there is some response in the ranges from 390 to 430 nm and from 675 to 720 nm, it is still notably limited (<10% of the peak color response) so that these wavelengths do not contribute significantly to our overall perception of color, even though we can see them if bright enough. This is reflected in the wavelength cutoff of the uniform chromaticity diagram in Figure 1. Any further reduction in this spectral cutoff, however, quickly diminishes the CRI, imparting a substantial visual impact (colored tinting) and reducing the level of transparency <99.5%. Similarly, any absorption "peak" centered in the visible, particularly near the photopic maximum, results in significant colored tinting as well more dramatic reductions in CRI and VT as outline by Eqs. (1) and (2).

Integrating the solar energy flux, there is approximately 8.6% in the UV (300–435 nm), 35.0% in the VIS (435 nm –670 nm), and 56.4% in the NIR (670–3000 nm), while for

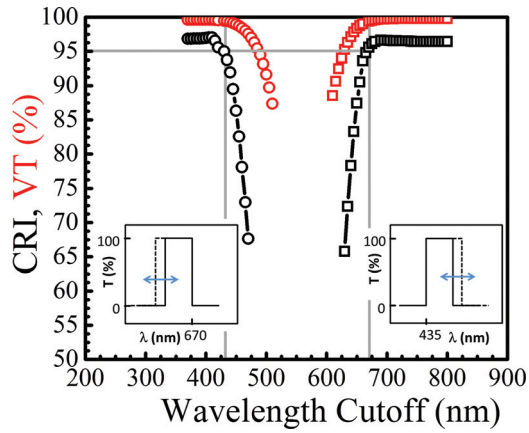

FIG. 2. Calculated CRI (black) and weighted VT (red) as a function of the low (circles) and high (squares) idealized visible transmission wavelength cutoff shown schematically inset. The two fixed wavelengths on each side were iterated to find the largest visible range that resulted in a CRI > 95 (corresponding VT > 99.5%). The range of visible light is, therefore, defined as 435–670 nm for the efficiency calculations.

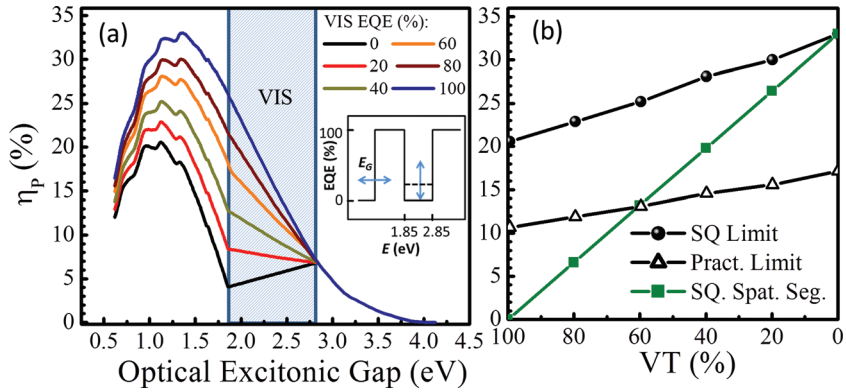

FIG. 3. (a) Calculated thermodynamic limiting efficiencies for single-junction (single-bandgap) photovoltaics as a function of bandgap for transparent and semitransparent architectures with varied EQE contributions from the visible part of the spectrum. Note that the decrease in efficiency through the visible region for 0% VIS EQE (black line) stems from the reduced open-circuit voltage combined with the lack of additional photocurrent. (b) Maximum single-junction efficiencies as a function of the total level of visible transparency in the SQ thermodynamic (closed circles), practical (open triangles), and SQ spatially segmented visibly opaque (closed squares) junction limits. The corresponding relationship between the visible EQE contribution and weighted VT can be approximated by EQE + VT = 1 in the absence of reflection losses.

the solar photon flux, there is 3.9% in the UV, 22.6% in the VIS, and 73.5% in the NIR. This indicates that there is substantial potential for both single- and multi-junction transparent solar cells that harvest primarily UV and NIR photons. For single-junction solar cells in the absence of multi-exciton generation processes, it is photon flux that is important (rather than energy flux) since every photon produces one excited state that thermally relaxes to the band edge. For multi-junction cells, it is the total energy flux that is more significant since multiple junctions act to reduce these thermal relaxation losses. In this case, the total potential solar cell efficiency loss in avoiding visible photon harvesting will be slightly greater with multi-junction cells than with single-junction cells.

Shown in Figure 3 is a plot of the thermodynamic efficiency limit as a function of bandgap for a range of EQEs from visible light spanning zero contribution (100% transparency) to 100% contribution (0% transparency, standard SQ limit). The peak efficiency and EQE as a function of the weighted VT is shown in Fig. 1(b) where no optical losses are assumed so that the relationship between the EQE and transmission is $\mathrm{EQE}(\lambda) + T(\lambda) = 1$. With increasing transparency, the maximum single-junction efficiency is modestly reduced from 33.1% to 20.6%, and the optimal bandgap becomes slightly redshifted from 1.36 eV to 1.12 eV. For comparison, the thermodynamic limit of spatially segmented PVs (i.e., a semi-transparent assembly of visibly opaque cells) is included in Fig. 3(b) highlighting the importance of harvesting non-visible photons in the high VT regime. In practice, the idealized EQE profiles (shown in inset 2(a) and 3(a)) can be closely approximated via various combinations of excitonic semiconductors (donor, acceptor, and/or blended donors and acceptors) or through combinations with excitonic materials and spatially segmented inorganic PVs.[2–4] Sharp transitions at the NIR and UV limits can, in part, be realized with optical layers such as low-E coatings already applied on windows or distributed Bragg reflectors, when combined with selectively UV/NIR-absorbing active layers.[2,36]

This analysis is extended to multi-junction cells connected in series in Figure 4 where the efficiency of single-junction cells with 100% VT increases from 20.5% to 27.1%, 29.8%, and 36.6% for 2, 3, and 16 junctions, respectively. The efficiency enhancement in going to an infinite number of multi-junction-tandem for 0% and 100% transparency is 1.98 and 1.85, paralleling the difference between the integrated photon and the energy solar flux. That is, the total enhancement in going to multi-junction transparent solar cells is reduced by approximately 15% over opaque cells since there is less integrated power flux in the UV and NIR parts of the spectrum than in the photon flux. In the practical limit, single-junction efficiencies (including optical losses)

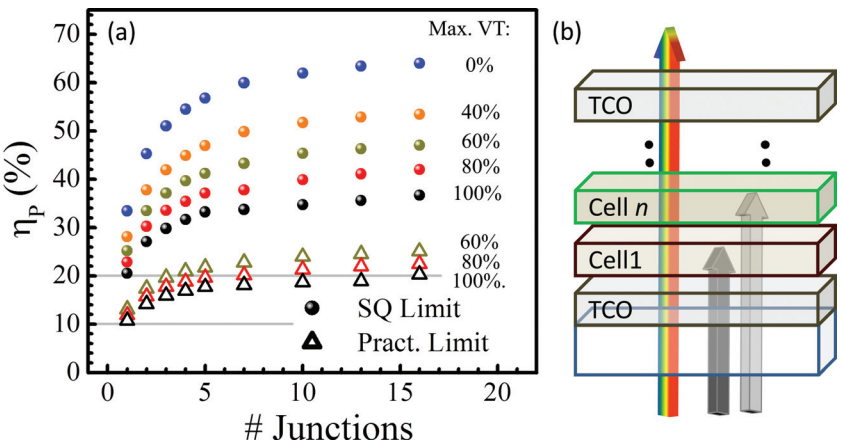

FIG. 4. (a) Calculated thermodynamic (closed circles) and practical junction (open triangles) efficiency limits for photocurrent-matched, series-integrated, multi-junction transparent solar cells as a function of the number of junctions for a range of visible EQE contributions (as labeled with the corresponding VT). (b) Schematic of the series-integrated, multi-junction photovoltaics.

with transparencies of 100% (60%) increase from 10.8% (14.6%) to 20.3% (29.6%) for 16 junctions. Fully accounting for optical losses, a more realistic transmission of ~80% should be associated with the curve for 0% VIS EQE contribution in Fig. 4 where optical losses are typically ~20%, including substrate reflections of ~5%–10%, interface reflections of ~5%–10%, and electrode absorption of ~5%–10%.

This work provides a guide for the ultimate and practical laboratory efficiency limits for visibly transparent photovoltaics architectures for applications with both stringent and relaxed transparency requirements. Transparent excitonic PV architectures with power production from ultra-violet and near-infrared photons have the potential to exhibit theoretical and practical single-junction efficiencies of 21% and 11%, respectively, while leaving the visible part of the spectrum unaffected. Widespread window adoption will require average transmission $\geq$60% placing the thermodynamic and realistic multi-junction efficiency limits at 47% and 23%, respectively (including small contributions from visible photons). A variety of schemes can further boost these efficiencies with greater partial photocurrent from visible photons for niche semitransparent and color-tinted applications. By focusing on developing thin-film excitonic molecules for photovoltaic architectures with selective absorption in the NIR and UV part of the spectrum, highly efficient and highly transparent energy harvesting surfaces will become a viable route to ubiquitous PV deployment and increased building efficiency.

The author thanks Vladimir Bulović and Miles C. Barr for many stimulating discussions.

[1]C. Tuchinda, S. Srivannaboon, and H. W. Lim, J. Am. Acad. Dermatol. **54**, 845 (2006).
[2]R. R. Lunt and V. Bulovic, Appl. Phys. Lett. **98**, 113305 (2011).
[3]R. Kuhn, A. Boueke, A. Kress, P. Fath, G. P. Willeke, and E. Bucher, IEEE Trans. Electron Devices **46**, 2013 (1999).
[4]K. Taira and J. Nakata, in *Solar Building Skins, Conference Proceedings of the 6th Energy Forum* (Economic Forum, Bressanone, Italy, 2011).
[5]P. Fath, H. Nussbaumer, and R. Burkhardt, Sol. Energy Mater. Sol. Cells **74**, 127 (2002).
[6]R. F. Bailey-Salzman, B. P. Rand, and S. R. Forrest, Appl. Phys. Lett. **88**, 233502 (2006).
[7]R. Koeppe, D. Hoeglinger, P. A. Troshin, R. N. Lyubovskaya, V. F. Razumov, and N. S. Sariciftci, ChemSusChem **2**, 309 (2009).
[8]Q. F. Dong, Y. H. Zhou, J. N. Pei, Z. Y. Liu, Y. W. Li, S. Y. Yao, J. B. Zhang, and W. J. Tian, Org. Electron. **11**, 1327 (2010).
[9]J. E. Lewis, E. Lafalce, P. Toglia, and X. Jiang, Sol. Energy Mater. Sol. Cells **95**, 2816 (2011).
[10]F. Li, S. Ruan, Y. Xu, F. Meng, J. Wang, W. Chen, and L. Shen, Sol. Energy Mater. Sol. Cells **95**, 877 (2011).
[11]J. Meiss, T. Menke, K. Leo, C. Uhrich, W. M. Gnehr, S. Sonntag, M. Pfeiffer, and M. Riede, Appl. Phys. Lett. **99**, 043301 (2011).
[12]G. M. Ng, E. L. Kietzke, T. Kietzke, L. W. Tan, P. K. Liew, and F. R. Zhu, Appl. Phys. Lett. **90**, 103505 (2007).
[13]H. Schmidt, H. Flugge, T. Winkler, T. Bulow, T. Riedl, and W. Kowalsky, Appl. Phys. Lett. **94**, 243302 (2009).
[14]L. Shen, Y. Xu, F. Meng, F. Li, S. Ruan, and W. Chen, Org. Electron. **12**, 1223 (2011).
[15]C. Tao, G. Xie, F. Meng, S. Ruan, and W. Chen, J. Phys. Chem. C **115**, 12611 (2011).
[16]Y. Zhou, H. Cheun, S. Choi, W. J. Potscavage, Jr., C. Fuentes-Hernandez, and B. Kippelen, Appl. Phys. Lett. **97**, 153304 (2010).
[17]A. Colsmann, A. Puetz, A. Bauer, J. Hanisch, E. Ahlswede, and U. Lemmer, Adv. Energy Mater. **1**, 599 (2011).
[18]Y. Galagan, J. E. J. M. Rubingh, R. Andriessen, C. C. Fan, P. W. M. Blom, S. C. Veenstra, and J. M. Kroon, Sol. Energy Mater. Sol. Cells **95**, 1339 (2011).
[19]A. Manor, E. A. Katz, R. Andriessen, and Y. Galagan, Appl. Phys. Lett. **99**, 173305 (2011).
[20]J. Y. Lee, S. T. Connor, Y. Cui, and P. Peumans, Nano Lett. **8**, 689 (2008).
[21]L. B. Hu, H. S. Kim, J. Y. Lee, P. Peumans, and Y. Cui, ACS Nano **4**, 2955 (2010).
[22]L. B. Hu, H. Wu, and Y. Cui, MRS Bull. **36**, 760 (2011).
[23]S. Choi, W. J. Potscavage, and B. Kippelen, Opt. Express **18**, A458 (2010).
[24]C. J. M. Emmott, A. Urbina, and J. Nelson, Sol. Energy Mater. Sol. Cells **97**, 14 (2012).
[25]J. Liu, A. W. Hains, J. D. Servaites, M. A. Ratner, and T. J. Marks, Chem. Mater. **21**, 5258 (2009).
[26]E. F. Schubert, *Light-Emitting Diodes* (Cambridge University Press, New York, 2006).
[27]W. Shockley and H. J. Queisser, J. Appl. Phys. **32**, 510 (1961).
[28]R. R. Lunt, T. P. Osedach, P. R. Brown, J. A. Rowehl, and V. Bulovic, Adv. Mater. **23**, 5712 (2011).
[29]K. Vandewal, K. Tvingstedt, A. Gadisa, O. Inganas, and J. V. Manca, Nature Mater. **8**, 904 (2009).
[30]M. A. Faist, T. Kirchartz, W. Gong, R. S. Ashraf, I. McCulloch, J. C. de Mello, N. J. Ekins-Daukes, D. D. C. Bradley, and J. Nelson, J. Am. Chem. Soc. **134**, 685 (2012).
[31]T. Kirchartz, K. Taretto, and U. Rau, J. Phys. Chem. C **113**, 17958 (2009).
[32]L. Jan Anton Koster, S. E. Shaheen, and J. C. Hummelen, "Pathways to a New Efficiency Regime for Organic Solar Cells," Adv. Energy Mater. (in press).
[33]M. Gruber, J. Wagner, K. Klein, U. Hormann, A. Opitz, M. Stutzmann, and W. Brutting, "Thermodynamic Efficiency Limit of Molecular Donor-Acceptor Solar Cells and its Application to Diindenoperylene/C60-Based Planar Heterojunction Devices," Adv. Energy Mater. (in press).
[34]$1/Watt White Paper, U.S. Department of Energy, Available online, accessed May 1, 2011 at http://www1.eere.energy.gov/solar/sunshot/pdfs/dpw_white_paper.pdf.
[35]R. Tipnis, J. Bernkopf, S. J. Jia, J. Krieg, S. Li, M. Storch, and D. Laird, Sol. Energy Mater. Sol. Cells **93**, 442 (2009).
[36]Y. Galagan, M. G. Debije, and P. W. M. Blom, Appl. Phys. Lett. **98**, 043302 (2011).